Optimization of the snowflake divertor by means of EMC3-Eirene simulations and experiments

T. Lunt[1], G.P. Canal[2], B.P. Duval[2], Y. Feng[1], B. Labit[2], P. McCarthy[3], H. Reimerdes[2], W.A.J. Vijvers[2], M. Wischmeier[1] and the EUROfusion MST1 Team*

[1]*Max Planck Institute for Plasma Physics, Garching/Greifswald, Germany*

[2]*Centre de Recherches en Physique des Plasmas, EPFL, Lausanne, Switzerland*

[3]*Department of Physics, University College Cork, Cork, Ireland*

Introduction

Power exhaust is considered as one of the biggest challenges for the realization of a fusion reactor based on the divertor tokamak design [1]. In order to mitigate the heat flux density occurring near the divertor strike points (SP) the 'snowflake' (SF) configuration was proposed by Ryutov [2] and for the first time realized experimentally on TCV [3]. The SF configuration is characterized by two additional SPs and a second-order null point, where the poloidal magnetic field vanishes together with its spatial derivatives. Since it would require an infinitely accurate control of the toroidal currents, an *exact* SF cannot be achieved in the experiment, but only approximated by approaching a secondary X-point to the 'primary' one (that determines the boundary of the confinement region). Following the convention of Ryutov [4], we will speak of a 'snowflake plus' (SF^+), when the secondary X-point is located in the private flux region (PFR) of the primary separatrix and of a 'snowflake minus', when it is located in the common flux region (CFR). In Ref. [5] we reported on the first EMC3-Eirene simulations on SF^+ configurations compared to experiments. While the simulations predicted power fluxes to the secondary SPs of only about 1% of the input power (assuming constant perpendicular particle- and power diffusivities $D_\perp$ and $\chi_\perp$), about 10% were found experimentally, indicating an enhanced transport across the separatrix in the SF configuration.

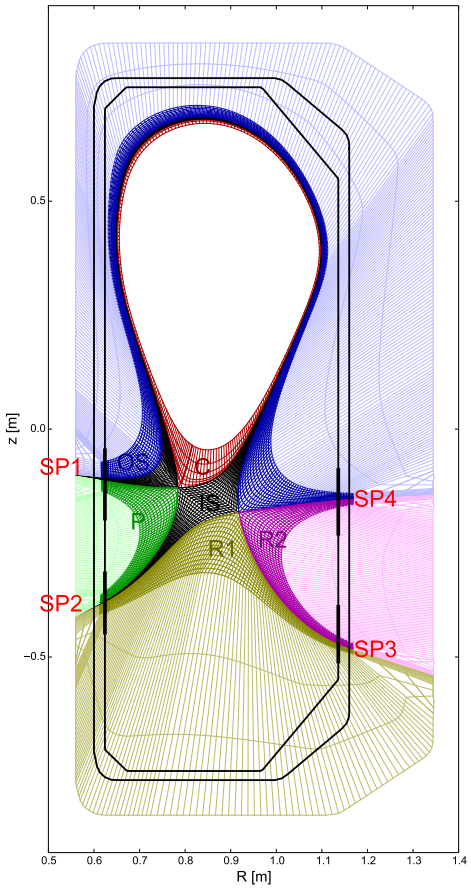

Figure 1: *Poloidal projection of the flux surface aligned computational grid for a LFS SF^- configuration with* $\rho_{x2} = 1.0075$.

*See http://www.euro-fusionscipub.org/mst1

If this transport is driven e.g. by β_{pol} instabilities as predicted by Ryutov [6] or if other mechanisms like drifts [7] are responsible needs to be investigated. As the power diffusing into the CFR is much larger than that to the PFR, a much larger power redistribution effect (combined with a reduction of the peak heat flux density at the primary targets) can be expected for a SF$^-$ without relying on this additional transport channel. Here we report on simulations including such configurations with the secondary X-point on the low-field side (LFS) of the primary one (LFS SF$^-$) with the goal of finding the optimum configuration. More details on these results can be found in Ref. [8]. Experimentally the SF$^-$ was investigated in Ref. [9].

Due to an in/out asymmetry observed experimentally [10] (for the favorable forward field conditions) in attached conditions and an asymmetric detachment [11], the outer target is loaded significantly stronger than the inner one for a single-null (SN) configuration and presently the limiting factor for the exhaustable power of the device. This asymmetry is often attributed to the drifts occurring in the SOL [12]. Another reason is the difference between connection lengths $L_{c,inner}$ and $L_{c,outer}$ from the outboard mid-plane (OMP) to the inner and outer targets respectively, as shown in Fig. 2 for the SN (green curves) in ASDEX Upgrade (AUG). Figure 2 also shows that $L_{c,outer}$ is significantly increased in the near-SOL region for a LFS SF$^-$ configuration computed for the realistic coil geometry but with currents that are presently beyond the tolerable force limits for AUG. If we assume that the detachment depends on L_c we can expect a detachment of the outer targets at significantly lower densities for the LFS SF$^-$.

Simulations

Plasma transport is simulated by the Edge Monte-Carlo 3D (EMC3) code that solves Braginskii's *fluid* equations, while EIRENE [13] solves the kinetic transport equation for the neutral particles. Both codes apply a Monte-Carlo technique to solve the equations. These equations and further details on the physics and the code coupling of the two codes can be found in Ref. [14]. Note that neither drifts, nor volumetric recombination are implemented in the code so far. An example of a computational grid used for the simulations is shown in Fig. 1. It comprises six zones, the confinement region (C), the inner (IS) and outer SOL (OS), the PFR (P) and the remote areas R1 and R2. Fig. 1 also shows the four SPs enumerated in counterclockwise direction starting from the inner target. In Ref. [8] parameters $\rho_{x2}, \vartheta_{x2}$ were intro-

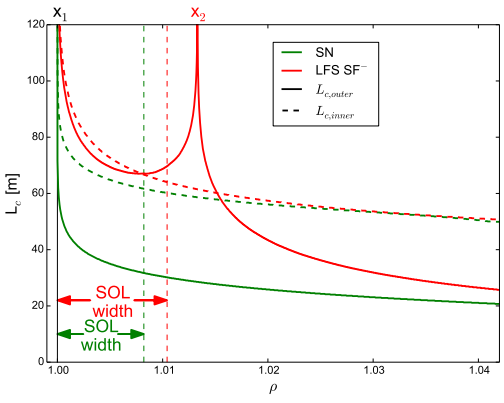

Figure 2: *Outboard mid-plane to inner ($L_{c,inner}$) and outer ($L_{c,outer}$) target connection length in AUG for a SN and a LFS SF$^-$ configuration.*

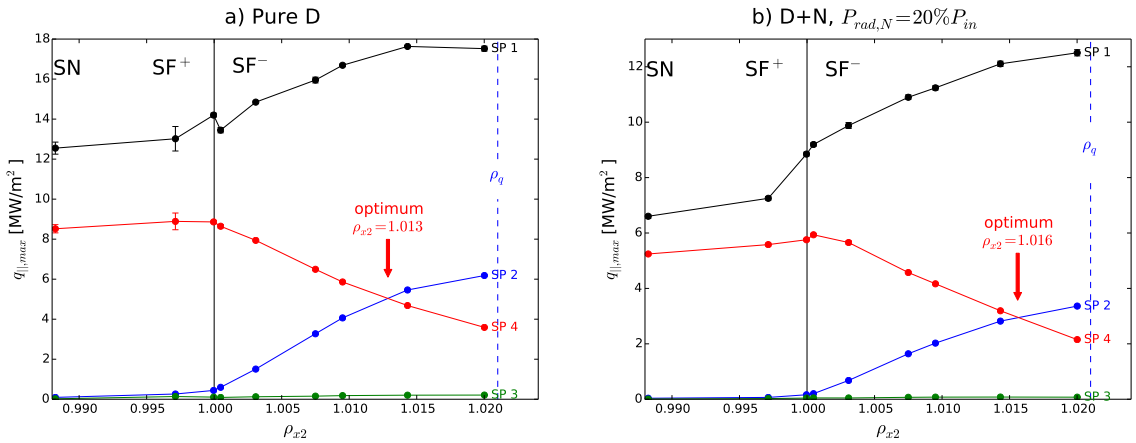

Figure 3: *Peak parallel power flux density $q_{||,max}$ near the different strike points SP 1... SP 4 for a series of nine simulations with different radial positions ρ_{x2} of the secondary X-point. The transport parameters were $D_\perp = 0.5$ m^2/s and $\chi_\perp = 1.5$ m^2/s. a) pure deuterium, b) with nitrogen radiating 20% of P_{in}.*

duced to classify the configuration, as an alternative to the parameters σ, θ used in Refs. [3, 5]. $\rho_{x2} = \left(\left(\Psi_{x2} - \Psi_o\right) / \left(\Psi_{x1} - \Psi_o\right)\right)^{0.5}$ is the radial coordinate, where Ψ_o is the poloidal magnetic flux on the magnetic axis and Ψ_{x1} and Ψ_{x2} those at the primary and secondary X-point, respectively. For reference, $\rho_{x2} < 1$ for the SF$^+$, $\rho_{x2} = 1$ for the exact SF and $\rho_{x2} > 1$ for the SF$^-$. ϑ_{x2} specifies the poloidal position of x_2 and is defined in Ref. [8]. All simulations were performed with deuterium as the main ion species, an input power of $P_{in} = 300$ kW equally distributed between the electrons and ions and a separatrix density at the OMP of $n_{OMP} = 1.5 \cdot 10^{19}$ m^{-3}, typical for medium density TCV discharges. The transport coefficients were chosen to be $D_\perp = 0.5$ m^2/s and $\chi_\perp = 1.5$ m^2/s and spatially constant to match typical target profiles.

Results

A series of nine configurations were simulated with ρ_{x2} covering the range of 0.988... 1.020. For $\rho_{x2} = 0.988$ the secondary X-point is far from the primary one and we refer to this case as the single-null (SN) reference. The upstream n_e and T_e profiles vary only by a few percent with ρ_{x2} and thus does the position $\rho_q = 1.021$ of the flux surface on which the power has fallen to 1/e of the separatrix value (cf. Fig. 7 in Ref. [8]). Fig. 3 shows the maximum parallel power flux density $q_{||,max}$ near the four strike points SP 1... SP 4 as a function of ρ_{x2}. Note that in contrast to the experimental observation $q_{||,max,SP_1}$ (black curve) is significantly larger than $q_{||,max,SP_4}$ (red). We attribute this discrepancy to the lack of drifts in the code and focus only on the outer SP 4 and SP 2 in the following[1]. From Fig. 3 a), $q_{||,max,SP_4}$ decreases monotonically with increasing ρ_{x2} for $\rho_{x2} > 1$ (the SF$^-$ case), while $q_{||,max,SP_2}$ increases. The configuration with $\rho_{x2} = 1.013$ where $q_{||,max,SP_2} = q_{||,max,SP_4}$ constitutes the one with the minimum load on the target and is thus

[1] Although SP 2 is located on the HFS, here we refer to it as an 'outer' SP for topological reasons.

considered optimal under the conditions considered so far. It was shown in Ref. [8] (Fig. 10) that (at least in attached conditions) this result depends only little on ϑ_{x2}.
Experimentally a similar effect was observed for the inner SP in a HFS SF$^-$ configuration in TCV, where a reduction of about 50% was found [15].
Figure 3 b) shows the same simulations as a) but with nitrogen impurities radiating a fixed amount of 20% of the input power. While the impurities radiate predominantly on the HFS for a SN and SF$^+$and therefore reduce $q_{||,max,SP_1}$, the fluxes to the outer SPs $q_{||,max,SP_2}$ and $q_{||,max,SP_4}$ are more affected for the LFS SF$^-$ where the impurities accumulate around the secondary X-point (cf. Fig. 12 in Ref. [8]). The radiation from carbon impurities was observed to be shifted to the LFS in a LFS SF$^-$ in the experiment.

Summary

A series of SN, SF$^+$ and LFS SF$^-$ configurations characterized by ρ_{x2} ranging from 0.988 to 1.020 was analyzed and simulated successfully by EMC3-Eirene. It was found that the maximum power flux density to the outer target can be reduced by a factor of two or presumably significantly more in a LFS SF$^-$ configuration due to three effects 1) a power splitting between SP 2 and SP 4 combined with steeper gradients and enhanced diffusion 2) an asymmetric irradiation of power removing predominantly power from the outer targets and 3) a longer connection length possibly facilitating the access to detachment at the outer targets.

Acknowledgement

This work has been carried out within the framework of the EUROfusion Consortium and has received funding from the Euratom research and training programme 2014-2018 under grant agreement No 633053. The views and opinions expressed herein do not necessarily reflect those of the European Commission.

References

[1] Zohm H. *et al.* 2013 *Nucl. Fusion* **53** 073019
[2] Ryutov D.D. *et al.* 2007 *Phys. of Plasmas* **14** 064502
[3] Piras F. *et al.* 2009 *Plasma Phys. Contr. Fusion* **51** 055009
[4] Ryutov D.D. *et al.* 2010 *Plasma Phys. Contr. Fusion* **52** 105001
[5] Lunt T. *et al.* 2014 *Plasma Phys. Control. Fusion* **56** 035009
[6] Ryutov D.D. *et al.* 2012 *Plasma Phys. Control. Fusion* **54** 124050
[7] Canal G. *et al.* 2015 *submitted to Nucl. Fusion*
[8] Lunt T. *et al.* 2015 *Submitted to Plasma Phys. Control. Fusion*
[9] Vijvers W.A.J. *et al.* 2015 *this conference*
[10] Eich T. *et al.* 2007 *Plasma Phys. Control. Fusion* **49** 573–604
[11] Potzel S. *et al.* 2014 *Nucl. Fusion* **54** 013001
[12] Aho-Mantila L. *et al.* 2012 *Nucl. Fusion* **52** 103006
[13] Reiter D. *et al.* 2005 *Fus. Sci. Tec.* **47** 172–186
[14] Feng Y. *et al.* 2004 *Contrib. Plasma Phys.* **44**, No. 1–3, 57–69
[15] Reimerdes H. *et al.* 2013 *Plasma Phys. Contr. Fusion* **55** 124027